TECHNICAL MEMORANDUM

X-475

INVESTIGATION OF EIGHT-STAGE BLEED-TYPE TURBINE FOR HYDROGEN-PROPELLED NUCLEAR ROCKET APPLICATIONS

I - DESIGN OF TURBINE AND EXPERIMENTAL PERFORMANCE OF FIRST TWO STAGES

By Harold E. Rohlik

Lewis Research Center
Cleveland, Ohio

NATIONAL AERONAUTICS AND SPACE ADMINISTRATION

WASHINGTON

May 1961

[redacted]

NATIONAL AERONAUTICS AND SPACE ADMINISTRATION

TECHNICAL MEMORANDUM X-475

INVESTIGATION OF EIGHT-STAGE BLEED-TYPE TURBINE FOR HYDROGEN-PROPELLED NUCLEAR ROCKET APPLICATIONS

I - DESIGN OF TURBINE AND EXPERIMENTAL PERFORMANCE OF FIRST TWO STAGES*

By Harold E. Rohlik

SUMMARY

Performance characteristics of the first two stages of an eight-stage turbine designed for the turbopump of a hydrogen-propelled nuclear rocket were investigated experimentally in cold hydrogen and in cold nitrogen. The turbine was designed for a blade-jet speed ratio of 0.110 and subsonic flow throughout. First-stage total efficiency when operating alone at the design blade-jet speed ratio of 0.284 was 0.67. Two-stage total efficiency at the design blade-jet speed ratio of 0.208 was 0.65 with 0.68 in the first stage and 0.61 in the second. The difference in stage efficiency resulted largely from lower reaction in the second stator.

No significant difference was found between efficiencies obtained in hydrogen and those obtained in nitrogen.

INTRODUCTION

A hydrogen-propelled rocket with a nuclear reactor heat source offers very high specific impulse and, consequently, low ratios of gross weight to payload for given missions. One turbopump system considered to provide the high pressures required for the thrust chamber of such a rocket is the bleed system, which utilizes a small fraction of the propellant flow to power the turbine. An analysis of turbopump characteristics for this system has been made and is reported in reference 1. This reference shows that the turbine will have a low blade-jet speed ratio because of the high-energy content of the pure hot hydrogen relative to the blade speeds available, which are limited by stress and temperature conditions. The blade-jet speed ratios associated with this application are in the neighborhood of 0.1. This means that large numbers of stages are required in

*Title, Unclassified.

order to obtain high turbine efficiency. In addition, the specific work required to pump liquid hydrogen is far higher than that for any other propellant because of the low density, so that high bleed rates, 2 to 4 percent, result. High turbine efficiency is therefore especially important to minimize bleed flow and the attendant loss in net specific impulse.

Detailed information on the performance of multistage turbines of this type is required to insure proper area matching of the blade rows so that all stages can deliver design work before limitations due to choking in the latter stages prevent adequate blade loading in the early stages. The most uncertain areas of information are the losses associated with the low blade heights in the early stages, leakage in the interstage seals, and their compounding effects on overall turbine performance.

In order to explore these problems, an eight-stage turbine with a blade-jet speed ratio of 0.11 was designed to drive a hydrogen pump with a flow rate of 100 pounds per second and a pressure rise of 1390 pounds per square inch. The turbine has been built; and the first two stages were tested in cold hydrogen and in cold nitrogen, in order to evaluate the effect of gas properties, at the Plumbrook Rocket Systems Research Facility.

This report presents the design of the eight-stage turbine and experimental performance of the first stage and the first two stages over a range of pressure ratios and speeds. Two-stage tests included two interstage seal geometries.

SYMBOLS

A_{ann} turbine-exit annular area, sq ft

c blade chord, in.

c_p specific heat at constant pressure, Btu/(lb)($^{\circ}$R)

D_p blade pressure-surface diffusion, $1 - \frac{V_i}{V_{min}}$

D_s blade suction-surface diffusion, $1 - \frac{V_{max}}{V_e}$

D_{tot} $D_s + D_p$

g acceleration due to gravity, 32.17 ft/sec^2

$\Delta h'$ turbine specific work, Btu/lb

J mechanical equivalent of work, 778.2 ft-lb/Btu

l passage height, in.

N rotative speed, rpm

n number of blades in row

p pressure, lb/sq ft

R gas constant, 766.5 in hydrogen, 55.16 in nitrogen, ft-lb/(lb)(^{o}R)

S_c untapered centrifugal stress, psi

s blade spacing, in.

T temperature, ^{o}R

U mean blade velocity, ft/sec

V absolute gas velocity, ft/sec

V_{cr} critical velocity, $\sqrt{\frac{2\gamma gRT'}{\gamma + 1}}$, ft/sec

V_j ideal jet speed corresponding to total-to-static pressure ratio,

$$\sqrt{2gJc_pT_i'\left[1 - \left(\frac{p_e}{p_i'}\right)^{\frac{\gamma-1}{\gamma}}\right]}$$

W gas velocity relative to rotor blade, ft/sec

W_{cr} critical velocity relative to blade, $\sqrt{\frac{2\gamma gRT''}{\gamma + 1}}$, ft/sec

w weight flow, lb/sec

α absolute gas flow angle measured from axial direction, deg

β relative gas flow angle measured from axial direction, deg

γ ratio of specific heats

δ ratio of inlet pressure to NACA sea-level pressure, $p_i'/2116.2$

ϵ function of γ used in relating weight flow to that at NACA standard atmosphere conditions,

$$0.740 \frac{1}{\gamma}\left(\frac{\gamma + 1}{2}\right)^{\frac{\gamma}{\gamma-1}}$$

η turbine efficiency based on inlet and exit total pressures

η_p pump efficiency

η_s turbine efficiency based on inlet total and exit static pressures

θ_{cr} squared ratio of turbine-inlet critical velocity to that of NACA standard sea-level atmosphere, $\left(\frac{V_{cr}}{1019}\right)^2$

ν blade-jet speed ratio, U/V_j

ρ_m blade metal density, lb/cu ft

Subscripts:

e exit

eq equivalent

i inlet

id ideal

max maximum

min minimum

r rotor

u circumferential component

x axial component

Superscripts:

' absolute total state

" relative total state

EIGHT-STAGE TURBINE DESIGN

Selection of a Design Point

The selection of a turbine design point requires examination of the effect of the turbine design on the rocket. The turbine in a bleed system influences the rocket gross weight through its weight as part of the structure and through its working fluid requirement that reduces the quantity of fluid available to develop thrust in the rocket chamber and nozzle. These effects are discussed in reference 1 for a simple vertical mission determined to be equivalent to an earth satellite mission regarding rocket requirements. This reference reported results of an analytical investigation of bleed-type turbopump systems suitable for a high-pressure hydrogen-propelled nuclear rocket, and showed that rocket gross weight increased significantly with all turbopump systems investigated as the number of turbine stages was reduced below eight. An eight-stage design was therefore selected for the turbine of the subject investigation, and the following pump characteristics were assumed to determine the turbine power and speed requirements:

Pump type	axial flow
Rotative speed, N, rpm	47,800
Weight flow, w, lb/sec	100
Pressure rise, lb/sq in.	1390
Efficiency, η_p	0.7

The turbine was therefore required to produce 11,770 horsepower at 47,800 rpm. High values of turbine-inlet pressure and temperature, 1000 pounds per square inch and 1860° R, respectively, were selected to obtain a high value of turbine specific work. The turbine-exit area was determined as the maximum allowable from stress consideration for the same reason and corresponds to an untapered blade stress of 40,000 psi and a disk stress of 70,000 psi. With these inlet conditions and the maximum exit flow area, the eight-stage turbine design numbers are as follows:

Hydrogen weight flow, w, lb/sec	3.475
Specific work, $\Delta h'$, Btu/lb	2394
Mean blade speed, U, ft/sec	1420
Blade-jet speed ratio, ν	0.110
Static efficiency, η_s	0.72
Total-to-static pressure ratio, p_i'/p_e	12.68
Mean diameter, in.	6.81

The relation between work, speed, stage number, and turbine efficiency was taken from reference 2.

Velocity Diagrams

Velocity diagrams were computed for the mean diameter only, and the blades in all rows were made with constant profile from hub to tip. The calculation of the velocity diagrams required specification of work division among the stages, loss distribution in each stage, reaction across the rotors, and flow area distribution. Work was divided equally among the stages with a constant mean diameter. This results in a constant blade speed and nearly constant blade-jet speed ratio so that stage efficiencies should be about equal. A stage total efficiency of 0.69, corresponding to the overall total-to-static efficiency of 0.72, was computed. The first stator operates under conditions that are somewhat different from the other stators in that the inlet velocity is low with no whirl. It was assumed that the effect of this difference would be small, however, so the first-stage efficiency and pressure-loss design numbers were made the same as in all other stages. This value was used as the stage efficiency in computing the velocity diagrams. It was arbitrarily specified that each stator would take a 4-percent drop in total pressure and that all other stage losses occurred in the rotor.

The turbine was designed for some reaction across each rotor. This was done by specifying a 20-percent increase in relative circumferential velocity across the rotor, or

$$W_{u,re} = -1.2\, W_{u,ri}$$

Turbine flow area at the exit was determined from centrifugal stress considerations as noted previously and corresponds to an untapered centrifugal blade stress of 40,000 psi. The following relation was used:

$$S_c = \frac{\pi \rho_m}{259,200g} N^2 A_{ann}$$

The area in the first stage was determined by specifying a stator-exit flow angle α_3 of 75°. This angle was considered near the maximum allowable without incurring excess losses and resulted in the maximum blade height permissible with full admission. The stage-to-stage area variation was made so that the axial critical velocity ratio V_x/V_{cr} at the stator exit increased linearly with stage number. This area increase was taken entirely in the stator of each stage, with the inner and outer walls contoured as shown in figure 1. The velocity diagram values are shown in table I.

Blade Profiles

Blade inlet and exit angles for each blade row were calculated from the free-stream flow angles and selected blade leading- and trailing-edge thicknesses. This was done by assuming no change in tangential velocity or loss in total pressure between the free stream and a radial plane just inside the blade row. With the angles thus established, blade profiles were drawn with straight suction surfaces upstream of the inlet opening and downstream of the throat. Solidity and aspect ratio were estimated with information presented in reference 3. Blade surface velocities were then computed for the suction and pressure surfaces of the hub, mean, and tip sections according to the method presented in reference 4 and modified in reference 5. A limit of suction-surface diffusion D_s was set at 0.25 with a total diffusion D_{tot} of 0.65. When calculated diffusion values exceeded the limits in the first blade surface layout, subsequent trials were made with increased solidity and/or modified surface curvatures. An example of a final surface velocity distribution is given in figure 2, which shows critical velocity ratio against axial distance for the mean section of the fourth rotor. Final blade geometry numbers and surface coordinates are given in tables II and III, and a photograph of the eight-stage rotor is shown in figure 3.

Tip Clearance and Interstage Seals

The rotor tip clearance specified was 0.019 inch and was considered the minimum that would provide safe clearance at the high-temperature - high-speed design operation. It may be noted that the tip clearance of 0.019 amounts to more than 7 percent of the total passage height in the first stage. Reference 6 presents the effect of rotor tip clearance on performance of a single-stage turbine similar in size and blade-jet speed ratio. In that investigation turbine work was found to decrease linearly with increases in tip clearance in the 3 to 10 percent range. The rate of decrease was 1.8 percent of turbine work for 1.0 percent of passage height removed for tip clearance. This indicates a significant penalty in efficiency for the type of tip clearance geometry selected in this

design. An axial spacing of 0.050 inch between rotor and adjacent stator parts was determined from consideration of bearing clearances and differential thermal expansion between the rotating and stationary parts.

The interstage seal geometry selected consisted of rotating labyrinth disks mounted between rotor disks with a radial clearance of 0.003 to 0.004 between the rings of the seal and the inner diameter of the stator assembly. This is shown in figure 1. The inner surface of the stators was coated with aluminum oxide so that, if rubbing occurred because of stress, temperature, or eccentricity, the aluminum oxide coating would remove stock from the labyrinth rings, which were 0.010 inch thick.

FIRST- AND TWO-STAGE DESIGN PARAMETERS

The design parameters for the first stage and the first two stages operating together are listed in the following table. Weight flow and rotative speed, of course, are the same as for the complete turbine, while the other parameters shown depend on stage number.

Parameter	First stage	First two stages
Hydrogen weight flow, w, lb/sec	3.475	3.475
Specific work, $\Delta h'$, Btu/lb	299.25	598.50
Rotative speed, N, rpm	47,800	47,800
Pressure ratio, p_i'/p_e	1.323	1.722
Blade-jet speed ratio, ν	0.284	0.208
Total efficiency, η	0.689	0.695

The design turbine-inlet conditions of 1000 pounds per square inch gage and 1860° R in hydrogen result in the following parameters used to adjust design numbers to equivalent air:

$$\theta_{cr} = 51.22 \qquad \delta = 68.05$$

$$\sqrt{\theta_{cr}} = 7.157 \qquad \epsilon = 1.012$$

The relation used to determine equivalent pressure ratio is taken from reference 7 and is as follows:

$$\left(\frac{p_i'}{p_e}\right)_{eq} = \left\{1 - 0.1667\,\frac{\gamma+1}{\gamma-1}\left[1 - \left(\frac{p_e}{p_i'}\right)^{\frac{\gamma-1}{\gamma}}\right]\right\}^{-3.5}$$

The constants are functions of γ in standard air.

As noted in SYMBOLS, these parameters are referenced to NACA standard sea-level dry air. They were selected so that all experimental data could be reduced to a common standard regardless of gas or inlet gas conditions. Design parameters reduced to standard air are as follows:

Parameter	First stage	First two stages
Weight flow, $\frac{w\sqrt{\theta_{cr}}}{\delta}\epsilon$, lb/sec	0.370	0.370
Specific work, $\Delta h'/\theta_{cr}$, Btu/lb	5.84	11.68
Rotative speed, $N/\sqrt{\theta_{cr}}$, rpm	6679	6679
Pressure ratio, $(p_i'/p_e)_{eq}$	1.326	1.730
Blade-jet speed ratio, ν	0.284	0.208
Total efficiency, η	0.689	0.695

The numbers listed correspond to design-point testing in standard air and are equivalent to the actual design numbers in that internal critical velocity ratios and corresponding velocity diagram angles are approximately the same. It is assumed that efficiency is therefore also the same.

APPARATUS AND INSTRUMENTATION

The test facility used in the experimental investigation was the same as that described in reference 8 and consisted of an inlet ducting system with pressure controls, the turbine test section, and exit ducting that exhausted to the atmosphere through a pressure control system. Power was absorbed by an eddy-current cradled dynamometer that also served as a speed control. Figure 4(a) shows the physical arrangement of these parts in the test building, and figure 4(b) shows the three turbine configurations tested. The second and third configurations had seal diameters of 6.000 and 4.032 inches, respectively, with the same clearance.

The smaller seal was built for two-stage testing only, in order to investigate the effect of seal clearance area.

Turbine performance was determined from measurements of weight flow, speed, torque, inlet and exit static pressures, and inlet temperature. The details of these measurements are the same as described in reference 8.

EXPERIMENTAL PROCEDURE

Test data were recorded on magnetic tape during steady-state operation over a range of pressure ratios and rotative speeds. Turbine-inlet pressure was held nominally constant at 100 pounds per square inch absolute, and inlet temperature varied from 25° to 90° F depending on outside temperature and expansion within the gas storage vessels during a run. Inlet-total-to-exit-static pressure ratio was varied from 1.21 to 2.12 for first-stage operation and 1.25 to 3.75 for two-stage operation. Rotative speed was varied from 20 to 120 percent of design speed for operation in nitrogen and from 20 to 100 percent in hydrogen, in increments of 20 percent. The mechanical speeds, calculated for a turbine-inlet temperature of 52° F, corresponding to design equivalent speed were 6830 rpm in nitrogen and 25,457 rpm in hydrogen.

A larger number of operating points was recorded for operation in nitrogen than in hydrogen because of the difference in gas properties and the limited gas supplies available. With a given volume of gas supply and given values of turbine-inlet pressure and temperature, running time varies inversely with the square root of the gas constant. This means almost four times as much running time in nitrogen for each storage vessel.

Six test runs were made to obtain the data presented in this report, with three configurations tested in both gases. The three were:

(1) The first stage

(2) The first and second stages with the design seal geometry

(3) The first and second stages with a reduced seal diameter and the same seal clearance

RESULTS AND DISCUSSION

First-Stage Operation

The first stage was tested at five pressure ratios and speeds from 20 to 100 percent of design equivalent speed in 20-percent increments. These operating points resulted in a range of blade-jet speed ratios from 0.05 to 0.32. Figure 5(a) shows total efficiency against blade-jet speed ratio for operation in nitrogen. Turbine efficiencies based on total pressures at the inlet and exit were computed because in a multistage turbine the kinetic energy at the exits of all stages except the last is available to the next stage. The points plotted represent five pressure ratios but fall in a single curve within the accuracy of measurements made. This curve indicates a total efficiency of about 0.67 at the design first-stage blade-jet speed ratio of 0.284. This efficiency is somewhat lower than the efficiency used in the design, 0.69, to compute velocity diagram parameters and flow areas.

Figure 5(b) shows total efficiency plotted against blade-jet speed ratio for operation in hydrogen at three pressure ratios and speeds of 20, 40, 60, 80, 90, and 100 percent of design speed. Fewer points are shown here because of the reasons noted previously, and this figure serves to confirm the levels of efficiency measured in nitrogen. The curve on the figure is the curve shown on figure 5(a) faired through the nitrogen data. The points fall slightly above the curve in the low range of blade-jet speed ratio and agree well with the curve near the design value.

Figure 6 is a map of turbine performance determined from operation in nitrogen and presented in terms of equivalent specific work $\Delta h'/\theta_{cr}$ and weight-flow-speed parameter $\frac{wN}{\delta}\epsilon$ for contours of constant total-to-static pressure ratio, equivalent speed, and total efficiency. This composite plot was selected to show turbine performance because all important variables are plotted. It is possible, therefore, to easily observe the simultaneous variation in the performance parameters as pressure ratio and/or speed are varied. It may be noted that blade-jet speed ratio lines would, if plotted, radiate from the origin just as the efficiency contours do, since each efficiency contour approximately represents a single value of blade-jet speed ratio. Two points of interest are shown in the figure. The first point is simply the point with coordinates corresponding to the design values of specific work, weight flow, and speed. The experimentally determined design speed line lies to the right of this point because the turbine passed 4 percent more than design weight flow at design speed and pressure ratio.

The second point is the point at which design velocity diagrams are most nearly approached, and has a blade-jet speed ratio of 0.284, the

design value. This point is more important from a research standpoint because it establishes the efficiency level obtained at design aerodynamic operation. It occurs to the right of the first point because of the excess weight flow. The variation in weight flow with pressure ratio is indicated by the slope of the design speed line in figure 6 and is shown directly in figure 7 where equivalent weight flow is plotted against pressure ratio for several speeds. This figure is a cross plot of measured weight flows plotted against speed and was used in the preparation of figure 6. The design point lies well below choking weight flow on the design speed line because of the subsonic velocities used in the design.

Two-Stage Operation

Figure 8(a) shows the variation in total efficiency with blade-jet speed ratio for two-stage operation in nitrogen. Data plotted were obtained at six pressure ratios and a speed range of 20 to 120 percent of design equivalent speed. The curve faired through all data points falls below the design point with a value of about 0.65 at the design blade-jet speed ratio of 0.208. Two-stage efficiency was therefore 0.02 less than first-stage efficiency when operating at the design blade-jet speed ratios. This drop in efficiency was accompanied by a change in equivalent weight flow, indicating that the first stage was no longer operating at its design pressure ratio. The following table summarizes first-stage and two-stage performance at design speed and pressure ratios.

Parameter	First-stage operation	Two-stage operation
Pressure ratio, p_i'/p_e (design)	1.326	1.730
Blade-jet speed ratio, ν (design)	0.284	0.208
Equivalent weight flow, $\frac{w\sqrt{\theta_{cr}}}{\delta}\epsilon$, lb/sec	0.384	0.375
Equivalent specific work, $\Delta h'/\theta_{cr}$, Btu/lb	5.67	10.94
Total efficiency, η	0.67	0.65

The weight flow obtained with two stages at design speed and pressure ratio was used with working plots of weight flow, speed, work, pressure ratio, and efficiency to determine the operating point of the first stage as part of the two-stage unit at design speed and pressure ratio. The first-stage performance figures thus obtained were used with overall performance to determine the operating point of the second stage. The

following table shows performance values for both stages when operating together at design speed and overall total-to-static pressure ratio, with θ_{cr}, δ, and ϵ referenced to the inlet of the first stage:

Parameter	First stage	Second stage
Pressure ratio, p_i'/p_e	1.299	1.353
Blade-jet speed ratio, ν	0.296	0.283
Equivalent weight flow, $\frac{w\sqrt{\theta_{cr}}}{\delta}\epsilon$, lb/sec	0.375	0.375
Equivalent specific work, $\Delta h'/\theta_{cr}$, Btu/lb	5.63	5.31
Total efficiency, η	0.68	0.61

The difference in blade-jet speed ratios between the first and second stage could account for a difference of about 0.017 in efficiency from aerodynamic loading considerations according to the curve of figure 5. The remaining 0.05 difference in efficiency must therefore result from the difference in stator operation, since the rotor blading and clearances were essentially the same for both stages.

A comparison of first and second stator losses made with two-stage performance data showed that losses in the second stator were approximately twice as great as those in the first. Reference 9 relates turbomachine losses to boundary-layer characteristics, and in figure 11 of the reference momentum thickness is shown as a function of blade row reaction with reaction defined as $1 - (V_i/V_e)$. The reference also relates blade row loss to momentum thickness and blade row geometry. The first and second stators of the eight-stage turbine have reaction values of 0.78 and 0.55, respectively, and these result in momentum thicknesses that were used with blade geometry to estimate blade losses. The estimates based on boundary-layer characteristics also show that second stator losses are approximately twice as great as first stator losses. This indicates that the difference between first and second stator performance is largely the result of the difference in blade row reaction.

Other differences in stator operation that also contributed to the greater losses in the second stator were incidence and interstage seal leakage. Measurements of exit flow angle made near design speed and pressure ratio indicate that the second stator had an inlet incidence angle of about 5.5°. At the kinetic-energy level existing, this could account for a loss of only 0.006 in efficiency, assuming that the kinetic energy of the stator-inlet velocity component normal to the blade leading edge would be lost. The other factor that may adversely affect second stator

performance is leakage across the interstage seal, which permits part of the flow to bypass the stator passage and reenter the turbine at the inner wall between the second stator and second rotor. The seal clearance area was about 4 percent of the stator throat area with the same pressure differential as the stator, so the leakage loss should have been well under 0.03 in efficiency, depending on the effectiveness of the labyrinth.

Figure 8(b) shows total efficiency against blade-jet speed ratio for two-stage operation in cold hydrogen with the nitrogen curve from figure 8(a) plotted. The agreement between hydrogen and nitrogen data is good over the entire range of blade-jet speed ratio.

Figure 9 shows a map of turbine performance for operation of the first two stages in cold nitrogen. The point representing design aerodynamic operation, at design speed and pressure ratio, lies to the right and below the point of design equivalent specific work and design weight-flow-speed parameter. This occurs because of the excess weight flow and the lower-than-design efficiency. The weight flow in this case was 1.6 percent above the design value, while the efficiency was 0.65 compared with the design value of 0.695. The design operating points on the performance map are located in a region of relatively large gradients in all parameters shown. This results from the low subsonic velocity levels in the early stages of the turbine and the efficiency variation in the low range of blade-jet speed ratio. It indicates an appreciable range in operation, since design operation is not near limiting loading of the blade rows. It may be noted, however, from the velocity diagram parameters shown in table I that the critical velocity ratios increase progressively, stage by stage, through the turbine so that the margin between design operation and limiting loading is progressively smaller. The fact that experimentally determined efficiencies were lower than design efficiency means that this margin between design specific work and limiting work will be reduced still further in the latter stages.

The variation in total efficiency with blade-jet speed ratio for two-stage operation with the interstage seal clearance area reduced by one third is shown in figure 10. Data recorded for operation in nitrogen and hydrogen agree well over the entire range of blade-jet speed ratio. No difference in performance between the two seal geometries could be detected; this indicated that seal leakage losses could not be large. This result was expected because the decrease in clearance area amounted to only 1.3 percent of the second-stage throat area. The initial seal leakage must have been less than the areas indicated with negligible secondary effects, and therefore the difference between first- and second-stage efficiencies must be largely due to the differences in stator operation.

Examination of the turbine parts after operation with the original seal configuration indicated that rubbing had occurred between the labyrinth seal disk and the aluminum oxide coating on the inner diameter of the second stator with no damage to either part. A small clearance, such as that specified in the design of this seal, may therefore be used safely with an abrasive material on the stationary surface.

Testing of all three configurations showed no significant differences between performance in hydrogen and performances in nitrogen. This result was also observed in the investigation reported in reference 8, wherein two single-stage turbines were also tested in cold hydrogen and cold nitrogen.

SUMMARY OF RESULTS

An investigation was conducted to provide design information for turbines of the type required for the turbopump system of a hydrogen-propelled nuclear rocket. Performance characteristics of the first two stages of an eight-stage turbine for this application were obtained experimentally in cold nitrogen and in cold hydrogen to establish the effects of fluid properties on turbine performance. Results of this investigation may be summarized as follows:

1. Total efficiency of the first stage was 0.67 when operating alone at its design blade-jet speed ratio of 0.284. Measured equivalent weight flow was 4 percent higher than the design value.

2. Total efficiency obtained for operation of the first two stages was 0.65 at the design blade-jet speed ratio of 0.208. The equivalent weight flow for two-stage operation was 1.4 percent above the design value.

3. Calculations made with two-stage performance data at design operation showed that the first-stage efficiency was 0.68, second efficiency was 0.61, and that the difference resulted largely from boundary-layer losses in the stators. The second stator losses were approximately twice as large as first stator losses according to experimental performance data and also according to estimated losses based on boundary-layer calculations.

4. Tests made with a one-third reduction in interstage seal leakage area showed no measurable difference in efficiency, so seal leakage losses must have been small.

5. Operation in hydrogen and nitrogen showed no significant differences between the two gases in the levels of efficiency obtained.

6. It was found that rubbing occurred with material removed from labyrinth rings by abrasive with no damage to either part. It was concluded therefore that seal clearances of 0.003 to 0.004 inch may be safely used with an abrasive coating on the side opposite the labyrinth.

Lewis Research Center
National Aeronautics and Space Administration
Cleveland, Ohio, February 7, 1961

REFERENCES

1. Rohlik, Harold E., and Crouse, James E.: Analytical Investigation of the Effect of Turbopump Design on Gross-Weight Characteristics of a Hydrogen-Propelled Nuclear Rocket. NASA MEMO 5-12-59E, 1959.

2. Stewart, Warner L.: Analytical Investigation of Multistage-Turbine Efficiency Characteristics in Terms of Work and Speed Requirements. NACA RM E57K22b, 1958.

3. Miser, James W., Stewart, Warner L., and Whitney, Warren J.: Analysis of Turbomachine Viscous Losses Affected by Changes in Blade Geometry. NACA RM E56F21, 1956.

4. Stewart, Warner L., Wong, Robert Y., and Evans, David G.: Design and Experimental Investigation of Transonic Turbine with Slight Negative Reaction Across the Rotor Hub. NACA RM E53L29a, 1954.

5. Miser, James W., Stewart, Warner L., and Monroe, Daniel E.: Effect of High Rotor Pressure-Surface Diffusion on Performance of a Transonic Turbine. NACA RM E55H29a, 1955.

6. Kofskey, Milton G.: Experimental Investigation of Three Tip-Clearance Configurations over a Range of Tip Clearance Using a Single-Stage Turbine of High Hub- to Tip-Radius Ratio. NASA TM X-472, 1961.

7. Heaton, Thomas R., Slivka, William R., and Westra, Leonard F.: Cold-Air Investigation of a Turbine with Nontwisted Rotor Blades Suitable for Air Cooling. NACA RM E52A25, 1952.

8. Wong, Robert Y., and Darmstadt, David L.: Comparison of Experimentally Obtained Performance of Two Single-Stage Turbines with Design Ratios of Blade to Jet Speed of 0.191 and 0.262 Operated in Hydrogen and Nitrogen. NASA TM X-415, 1961.

9. Stewart, Warner L., Whitney, Warren J., and Wong, Robert Y.: A Study of Boundary Layer Characteristics of Turbomachine Blade Rows and Their Relation to Over-All Blade Loss. Paper 59-A-23, ASME, 1960.

TABLE I. - MEAN-SECTION FREE-STREAM VELOCITY DIAGRAM PARAMETERS

(a) Stator exit

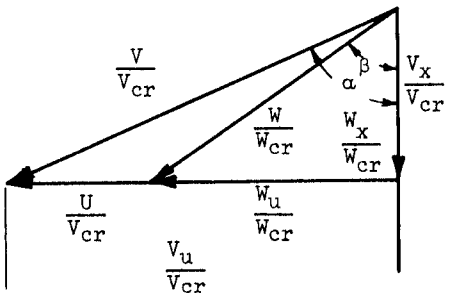

(b) Rotor exit

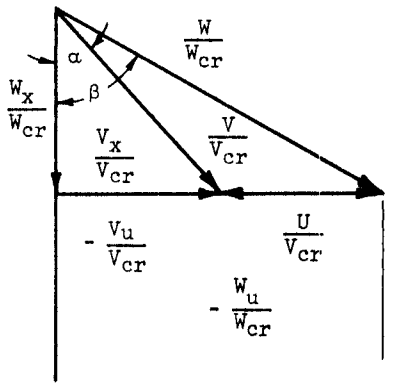

Stage	V/V_{cr}	V_x/V_{cr}	V_u/V_{cr}	α	U/V_{cr}	W/W_{cr}	W_x/W_{cr}	W_u/W_{cr}	β
1	0.541	0.140	0.523	75.0	0.195	0.361	0.141	0.332	67.0
2	.561	.169	.535	72.4	.199	.381	.171	.341	63.4
3	.583	.198	.548	70.1	.204	.403	.201	.353	60.1
4	.607	.227	.563	68.0	.209	.427	.231	.359	57.2
5	.632	.256	.578	66.1	.215	.452	.261	.369	54.7
6	.660	.285	.595	64.4	.221	.479	.292	.380	52.5
7	.689	.315	.614	62.9	.228	.507	.321	.392	50.7
8	.721	.344	.634	61.6	.236	.537	.351	.407	49.2

Stage	V/V_{cr}	V_x/V_{cr}	$-V_u/V_{cr}$	$-\alpha$	U/V_{cr}	W/W_{cr}	W_x/W_{cr}	$-W_u/W_{cr}$	$-\beta$
1	0.255	0.152	0.205	53.4	0.199	0.427	0.151	0.399	69.3
2	.279	.185	.210	48.6	.204	.448	.183	.409	65.9
3	.306	.218	.215	44.6	.209	.472	.216	.420	62.8
4	.336	.253	.221	41.2	.215	.498	.250	.431	59.9
5	.368	.289	.227	38.3	.221	.527	.285	.443	57.2
6	.402	.326	.235	35.8	.228	.559	.322	.457	54.8
7	.438	.365	.242	33.6	.236	.593	.360	.471	52.6
8	.477	.406	.251	31.7	.244	.631	.400	.488	50.7

TABLE II. - BLADE GEOMETRY

Stage	Number of blades, n	Blade chord, c, in.	Passage height, l, in.	Blade spacing, s, in.	Solidity, c/s	Aspect ratio, l/c
Stators						
1	93	0.333	0.268	0.230	1.45	0.81
2	116	.328	.280	.185	1.78	.85
3	112	.354	.304	.191	1.85	.86
4	106	.379	.342	.202	1.88	.90
5	100	.428	.400	.214	2.00	.94
6	104	.428	.481	.206	2.08	1.12
7	108	.455	.596	.198	2.30	1.31
8	106	.425	.765	.202	2.10	1.80
Rotors						
1	128	0.307	0.268	0.167	1.84	0.87
2	130	.353	.279	.165	2.14	.79
3	116	.366	.304	.185	1.98	.83
4	102	.440	.342	.210	2.10	.78
5	99	.468	.400	.216	2.16	.86
6	106	.458	.480	.202	2.27	1.05
7	110	.461	.596	.195	2.37	1.29
8	114	.428	.765	.188	2.28	1.79

E-1120

TABLE III. - BLADE COORDINATES

(a) Stators

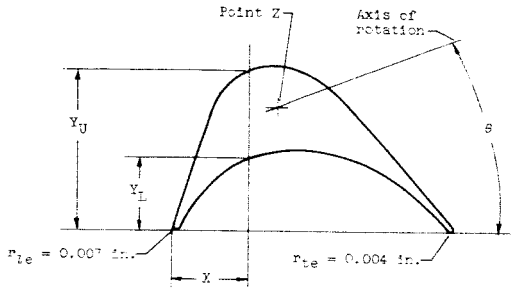

(The line of points Z is a radial line.)

X, in.	Y_L, in.	Y_U, in.	X	Y_L	Y_U	X	Y_L	Y_U	X	Y_L	Y_U
Point Z:	First stage X = 0.117, Y = 0.035 θ = 60°23'		Second stage Point Z: X = 0.131, Y = 0.114 θ = 21°37'			Third stage Point Z: X = 0.137, Y = 0.118 θ = 22°6'			Fourth stage Point Z: X = 0.151, Y = 0.117 θ = 22°40'		
0	0.011	0.011	0	0.007	0.007	0	0.0070	0.0070	0	0.0070	0.0070
.020	.004	.048	.025	.029	↕	.025	.0245	↕	.025	.0235	↕
.040	.017	.056	.045	-----	.141	.050	.0360		.050	.0350	
.060	.025	.063	.050	.060	.151	.053	------	.1355	.059	------	.1300
.080	.030	.063	.075	.077	.177	.075	.0800	.1675	.075	.0775	.1550
.100	.033	.061	.100	.088	.187	.100	.0945	.1837	.100	.0930	.1765
.120	.034	.057	.125	.094	.188	.125	.1035	.1935	.125	.1025	.1860
.132	-----	.054	.150	.095	.182	.150	.1082	.1975	.150	.1080	.1975
.140	.033	↑	.175	.093	.169	.175	.1085	.1962	.175	.1090	.1920
.160	.031		.200	.087	.148	.200	.1047	.1815	.200	.1070	.1690
.180	.029		.213	-----	.135	.225	.0967	.1580	.225	.1010	.1500
.200	.026		.225	.077	↕	.2295	------	.1335	.244	------	.1330
.220	.022	Straight	.250	.063		.250	.0845		.250	.0910	↕
.240	.018	line	.275	.045		.275	.0680	↕	.275	.0780	
.260	.015		.300	.022		.300	.0475		.300	.0610	
.280	.011	↕	.325	.004	.004	.325	.0240		.325	.0420	
.300	.006		.328			.354	.0040	.0040	.350	.0205	
.320	.002								.3795	.0040	.0040
.333	.004	.004									
Point Z:	Fifth stage X = 0.159, Y = 0.116 θ = 26°33'		Sixth stage Point Z: X = 0.156, Y = 0.108 θ = 27°15'			Seventh stage Point Z: X = 0.166, Y = 0.103 θ = 28°26'			Eighth stage Point Z: X = 0.183, Y = 0.095 θ = 27°27'		
0	0.0070	0.0070	0	0.0070	0.0070	0	0.0070	0.0070	0	0.0070	0.0070
.025	.0235	.0680	.025	.0225	.0870	.025	.0198	↕	.028	.0195	↕
.050	.0550	.1176	.050	.0525	.1056	.050	.0458		.050	.0461	
.075	.0763	.1566	.075	.0735	.1420	.0522	------	.1053	.0543	------	.0957
.100	.0915	.1739	.100	.0885	.1589	.075	.0645	.1341	.075	.0648	.1234
.125	.1019	.1819	.125	.0968	.1666	.100	.0783	.1511	.1000	.0780	.1402
.150	.1089	.1836	.150	.1050	.1687	.125	.0883	.1602	.125	.0870	.1483
.175	.1120	.1804	.175	.1078	.1655	.150	.0954	.1635	.150	.0927	.1507
.200	.1120	.1724	.200	.1074	.1578	.175	.0992	.1620	.175	.0949	.1460
.225	.1093	.1604	.225	.1042	.1460	.200	.1010	.1564	.200	.0945	.1410
.250	.1035	.1445	.250	.0954	.1308	.225	.1002	.1471	.225	.0915	.1307
.275	.0951	.1261	.275	.0896	.1135	.250	.0967	.1345	.250	.0861	.1168
.300	.0842	.1068	.300	.0785	.0960	.275	.0907	.1195	.275	.0784	.1012
.325	.0710	.0880	.325	.0653	.0785	.300	.0822	.1040	.2788	------	.1000
.350	.0557	.0690	.350	.0506	.0609	.3071	------	.0993	.300	.0688	↕
.375	.0385	.0502	.375	.0339	.0434	.325	.0715	↕	.325	.0570	
.400	.0204	.0311	.400	.0164	.0258	.350	.0595		.350	.0435	
.428	.0040	.0040	.428	.0040	.0040	.375	.0459		.375	.0285	
						.400	.0313		.400	.0130	
						.425	.0157		.4256	.0040	.0040
						.4548	.0040	.0040			

TABLE III. - Concluded. BLADE COORDINATES

(b) Rotors

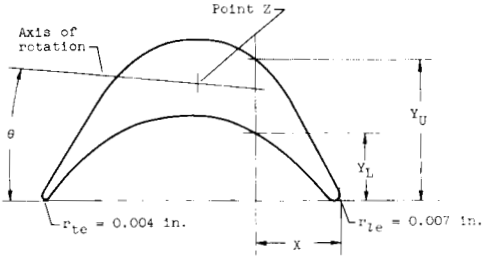

(The line of points Z is a radial line.)

X, in.	Y_L, in.	Y_U, in.	X	Y_L	Y_U	X	Y_L	Y_U	X	Y_L	Y_U
First stage Point Z: X = 0.146, Y = 0.117, θ = 3°31'			Second stage Point Z: X = 0.170, Y = 0.118, θ = 3°45'			Third stage Point Z: X = 0.1776, Y = 0.1286, θ = 2°[illegible]'			Fourth stage Point Z: X = 0.1838, Y = 0.1478, θ = 10°[illegible]'		
0	0.007	0.007	0	0.007	0.007	0	0.0070	0.0070	0	0.0070	0.0070
.025	.054	Straight	.025	.023	↕	.025	.0210	↕	.025	.0247	↕
.050	.052	line	.050	.041		.050	.0350		.050	.0505	
.063	-----	.142	.066	-----	.132	.075	.0765		.075	.0670	.1600
.075	.071	.159	.075	.070	.147	.081	-----	.1400	.100	.1040	.1928
.100	.083	.181	.100	.084	.170	.100	.0980	.1650	.125	.1175	.2100
.125	.091	.192	.125	.093	.185	.125	.1117	.1838	.150	.1270	.2192
.150	.094	.196	.150	.098	.192	.150	.1207	.1970	.175	.1340	.2225
.175	.093	.193	.175	.100	.193	.175	.1245	.2017	.200	.1365	.2207
.200	.088	.182	.200	.099	.190	.200	.1240	.2005	.225	.1347	.2135
.225	.077	.160	.225	.094	.180	.225	.1192	.1932	.250	.1307	.2017
.238	-----	.142	.250	.085	.163	.250	.1100	.1780	.275	.1237	.1840
.250	.061	↕	.275	.072	.139	.275	.0960	.1520	.300	.1135	.1604
.275	.038		.278	-----	.131	.281	------	.1427	.3205	------	.1365
.3066	.004	.004	.300	.054	↕	.300	.0760	↕	.325	.0935	↕
			.325	.027		.325	.0497		.350	.0820	
			.353	.004	.004	.350	.0155		.375	.0610	
						.3661	.0040	.0040	.400	.0367	
									.425	.0105	
									.440	.0040	.0040
Fifth stage Point Z: X = 0.1[illegible], Y = 0.1440, θ = 11°53'			Sixth stage Point Z: X = 0.1966, Y = 0.12[illegible], θ = 7°49'			Seventh stage Point Z: X = 0.1960, Y = 0.1261, θ = 10°13'			Eighth stage Point Z: X = 0.1826, Y = 0.1[illegible], θ = 8°27'		
0	0.0070	0.0070	0	0.0070	0.0070	0	0.0070	0.0070	0	0.0070	0.0070
.025	.0250	↕	.025	.0200	↕	.025	.0192	↕	.025	.0195	↕
.050	.0619		.050	.0494		.050	.0500		.050	.0466	
.075	.0890		.075	.0726		.075	.0760		.075	.0716	
.0765	------	.1620	.085	------	.1385	.0780	------	.150	.0797	------	.1167
.100	.1090	.1918	.100	.0905	.1593	.100	.0965	.1560	.100	.0855	.1430
.125	.1240	.2088	.125	.1040	.1800	.125	.1120	.1748	.125	.0997	.1570
.150	.1343	.2174	.150	.1144	.1924	.150	.1236	.1850	.150	.1065	.1650
.175	.1405	.2200	.175	.1212	.1967	.175	.1300	.1899	.175	.1104	.1667
.200	.1439	.2180	.200	.1249	.1967	.200	.1340	.1889	.200	.1115	.1665
.225	.1457	.2107	.225	.1255	.1900	.225	.1338	.1850	.225	.1095	.1594
.250	.1468	.1993	.250	.1230	.1792	.250	.1300	.1732	.250	.1057	.1479
.275	.1356	.1832	.275	.1178	.1709	.275	.1230	.1590	.275	.0960	.1320
.300	.1240	.1635	.300	.1098	.1567	.300	.1130	.1410	.300	.0832	.1120
.325	.1109	.1407	.325	.0987	.1368	.325	.1000	.1210	.3190	------	.0967
.338	------	.1288	.342	------	.1208	.3455	------	.104	.325	.0720	↕
.350	.0953	↕	.350	.0849	↕	.350	.0840	↕	.350	.0600	
.375	.0771		.375	.0683		.375	.0615		.375	.0508	
.400	.0569		.400	.0498		.400	.0436		.400	.0330	
.425	.0310		.425	.0265		.425	.0210		.4250	.0040	.0040
.450	.0114		.450	.0019		.450	.0037				
.4664	.0040	.0040	.47[illegible]	.0040	.0040	.4610	.0040	.0040			

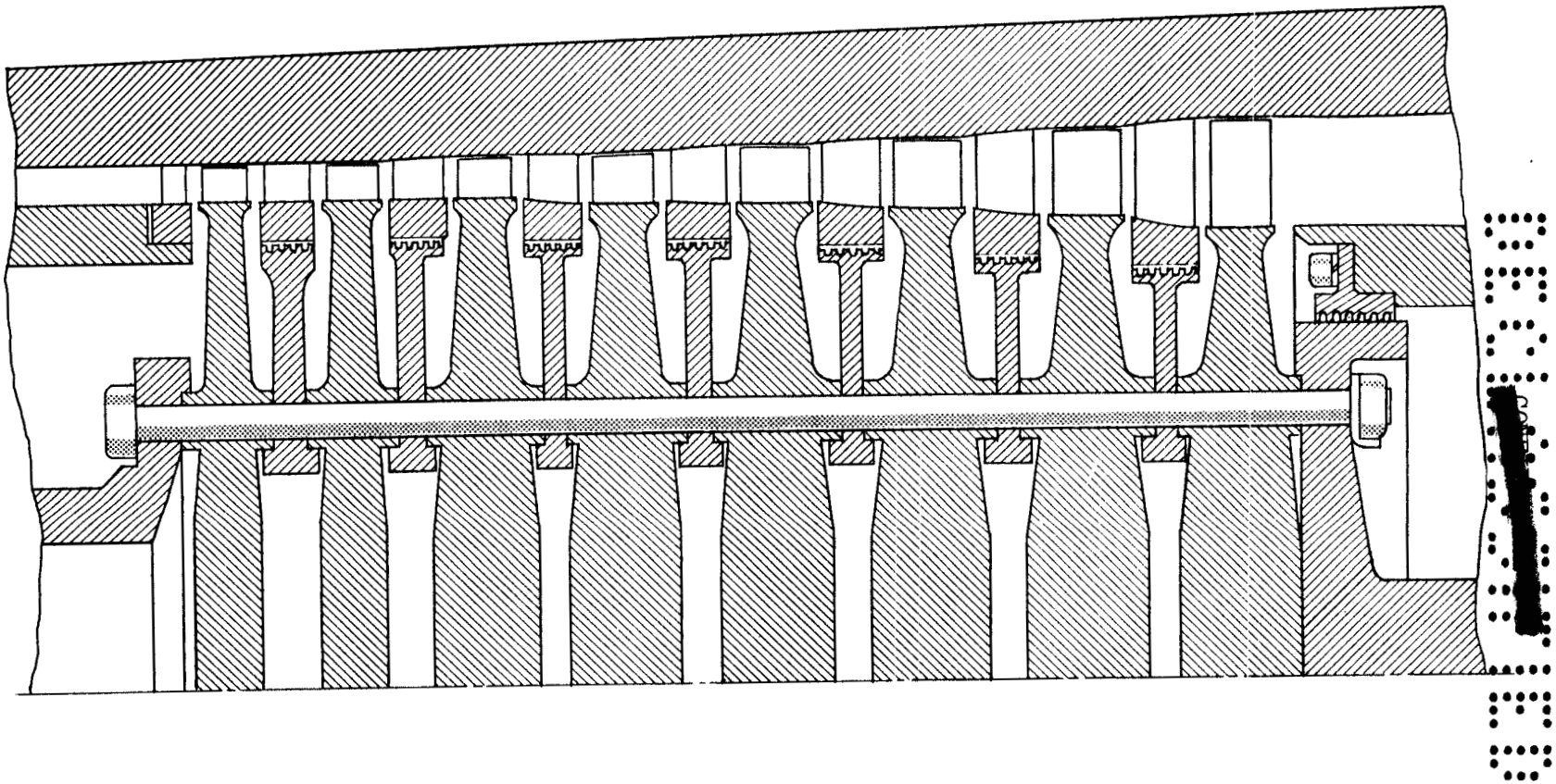

CD-7063

Figure 1. - Cross-sectional views of turbine through axis of rotation and blade rows through mean sections.

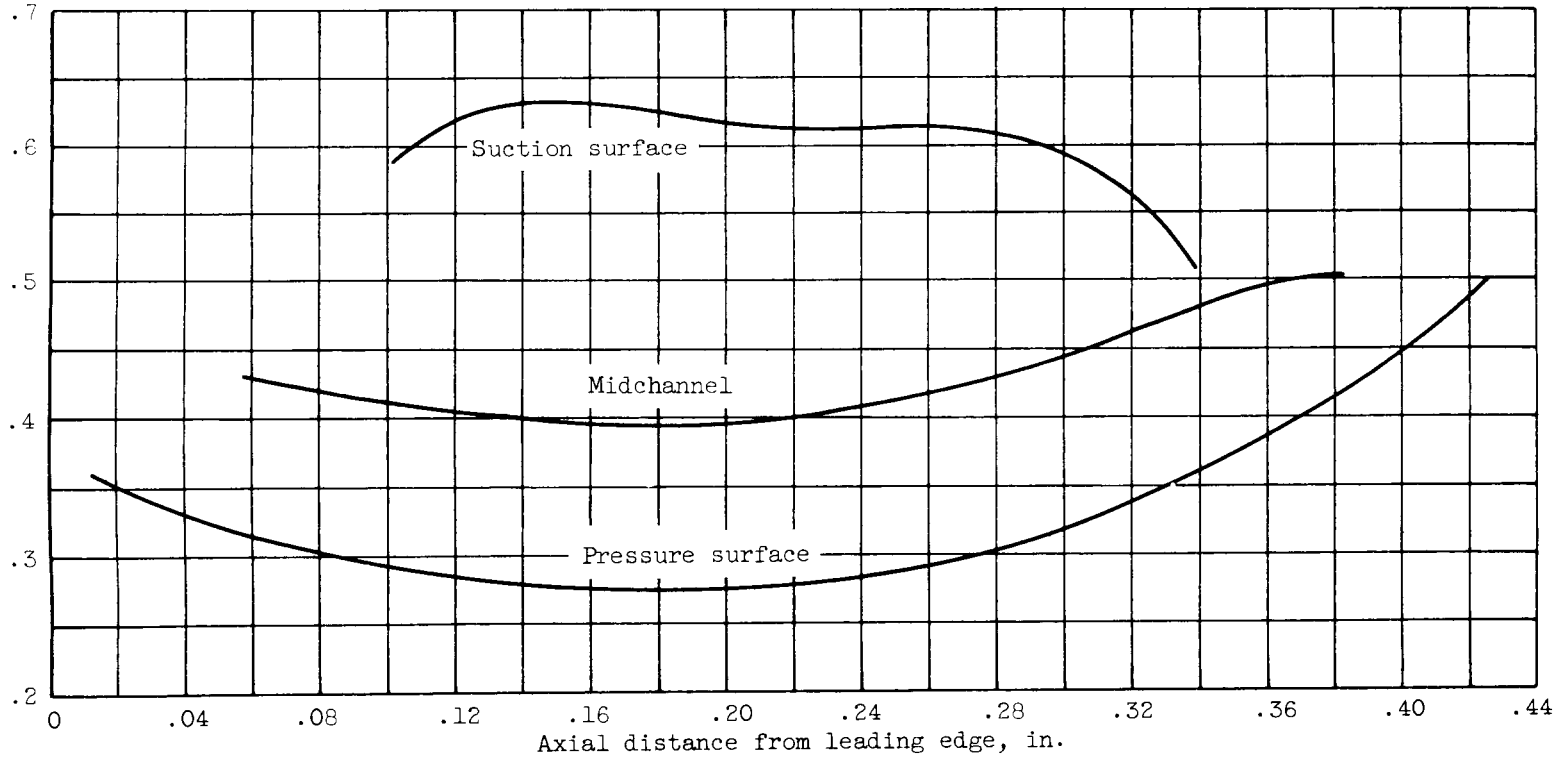

Figure 2. - Calculated channel velocities in fourth rotor at mean section.

Figure 3. - Eight-stage rotor.

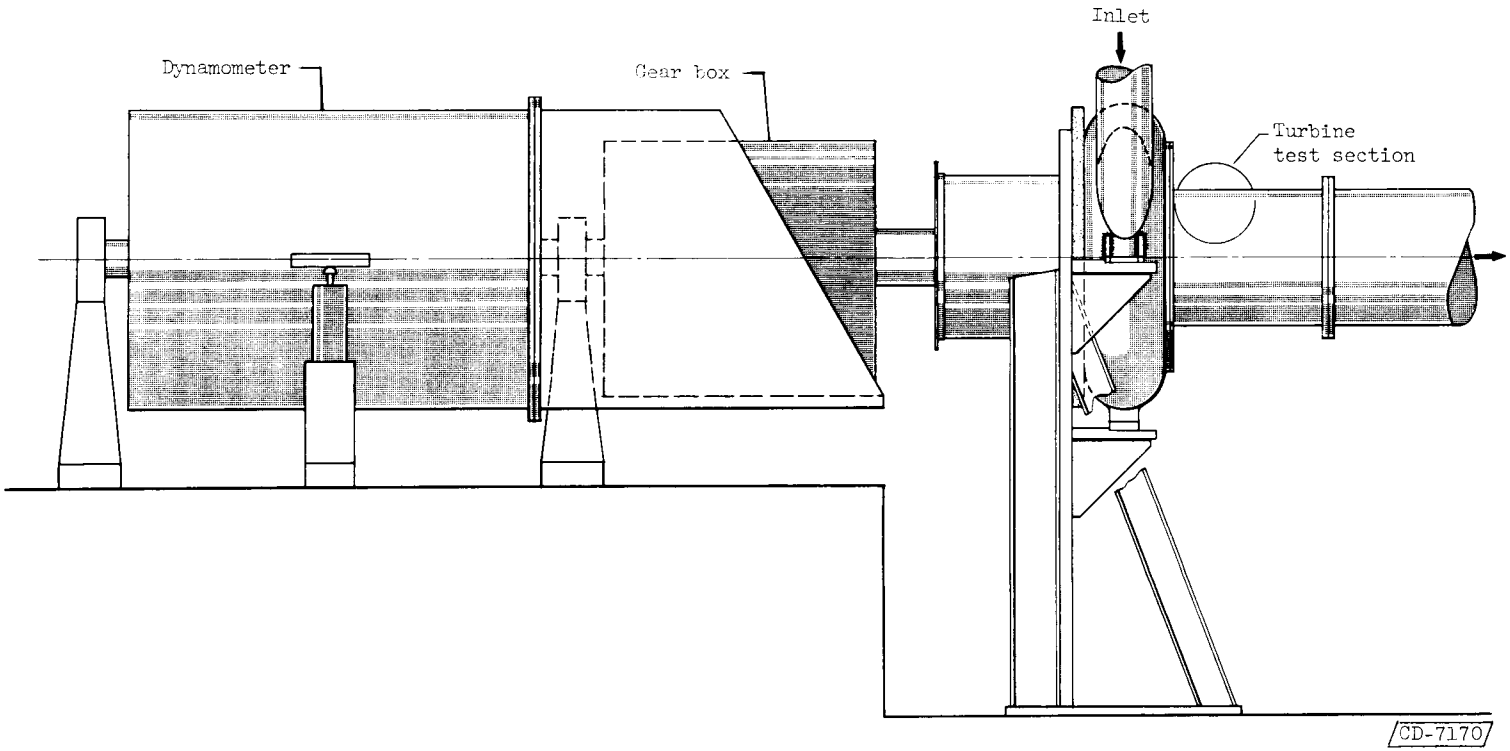

(a) Test facility.

Figure 4. - Test equipment.

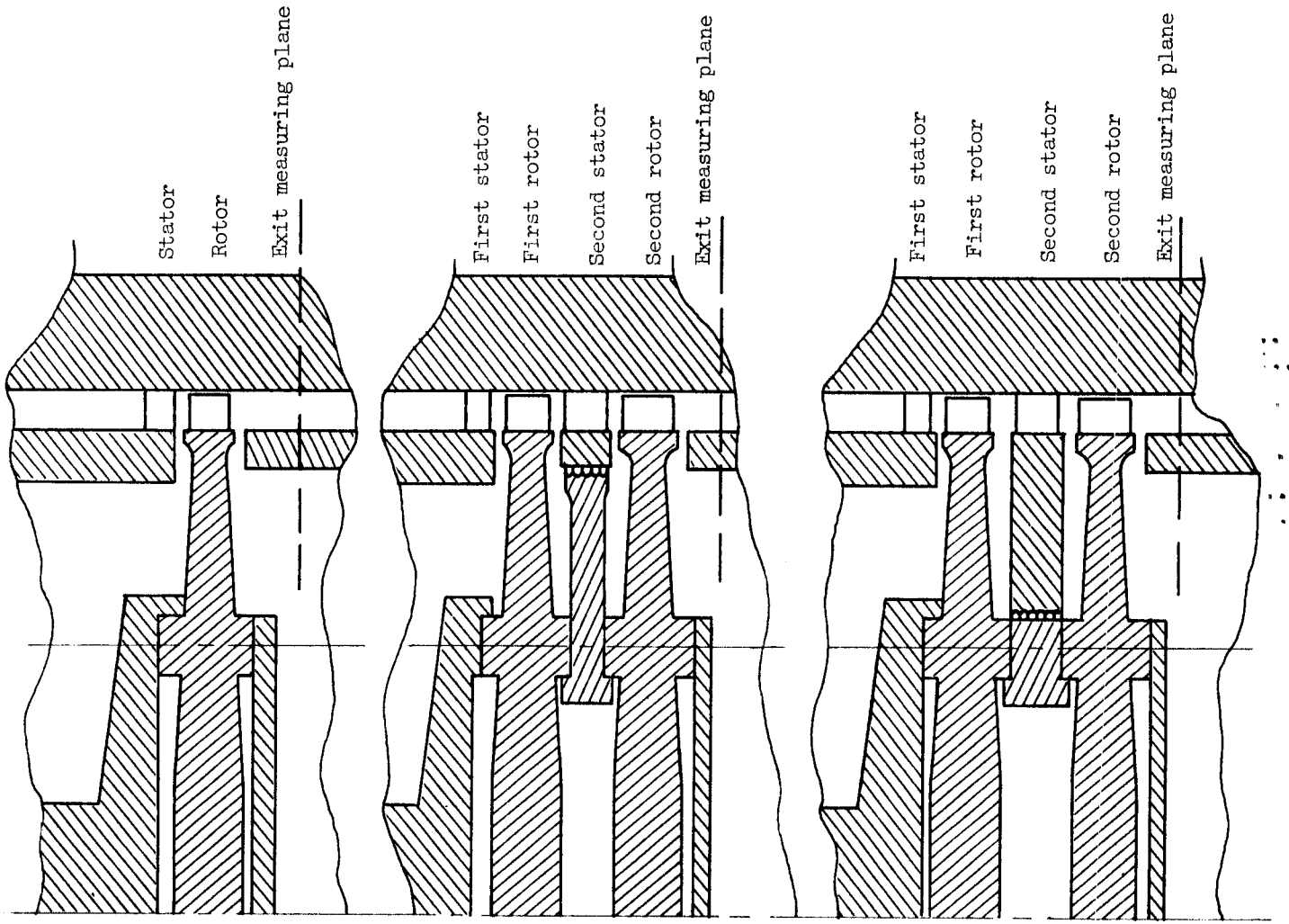

(b) Turbine blade and seal arrangements tested.

Figure 4. - Concluded. Test equipment.

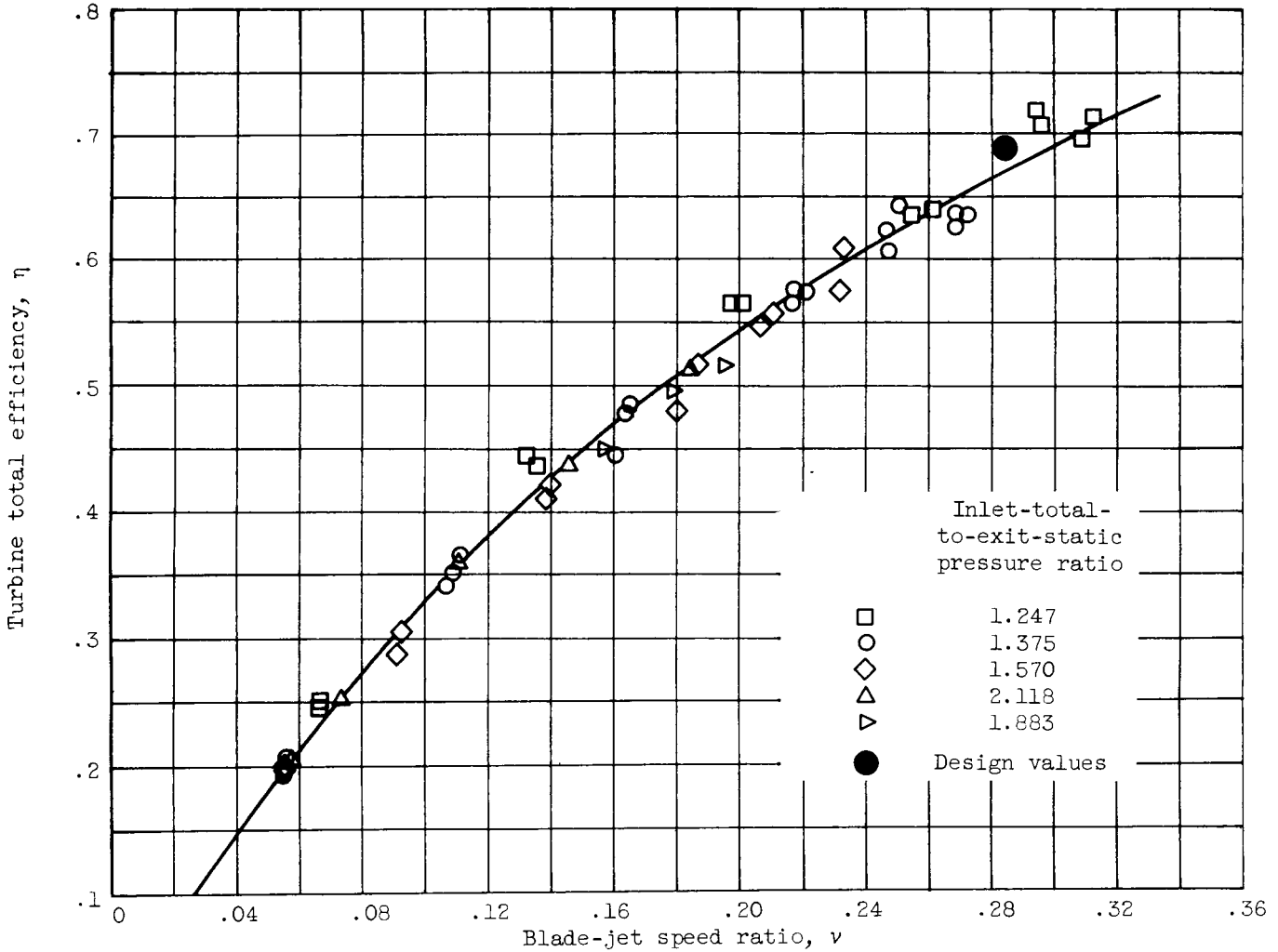

(a) In cold nitrogen.

Figure 5. - Turbine total efficiency variation for operation of first stage.

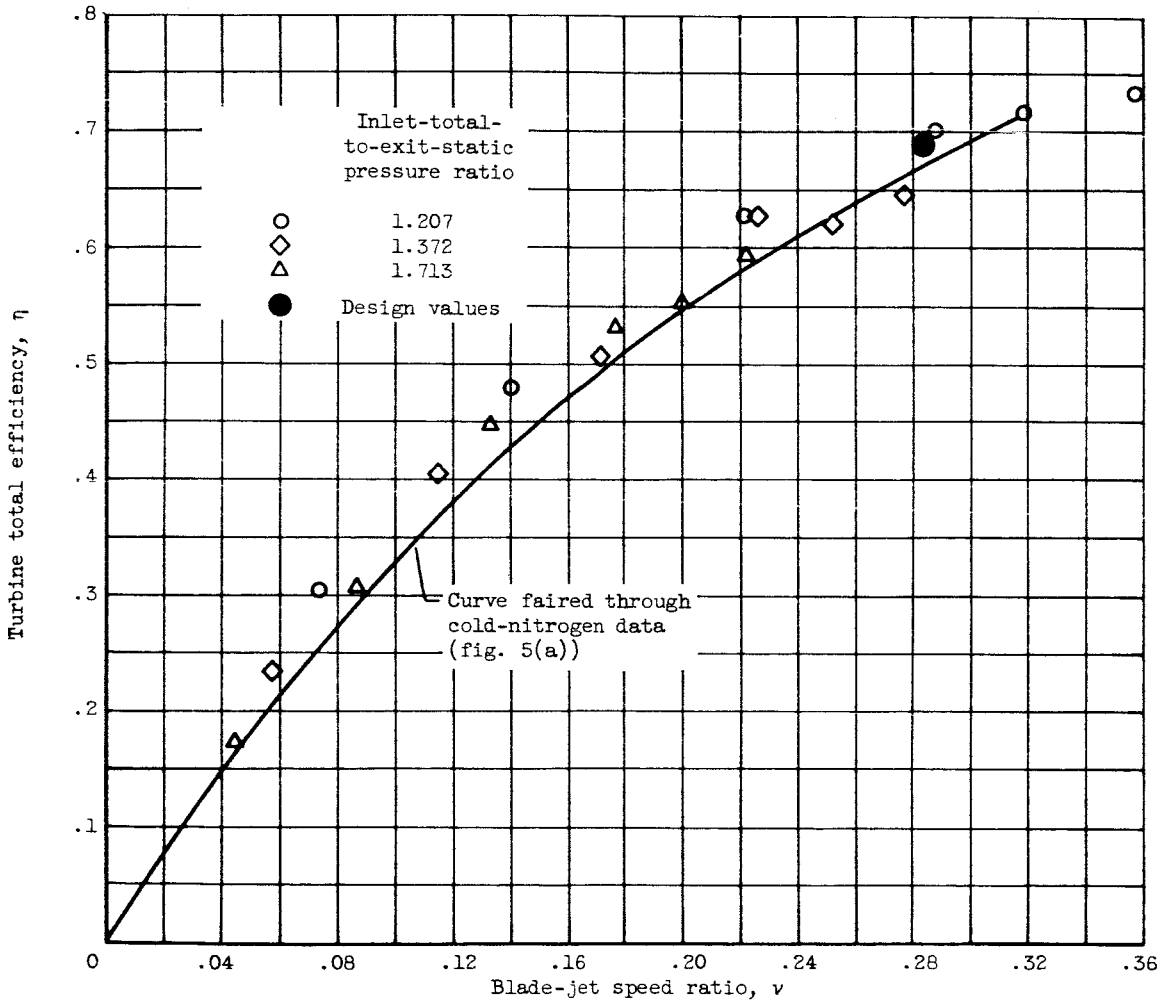

(b) In cold hydrogen.

Figure 5. - Concluded. Turbine total efficiency variation for operation of first stage.

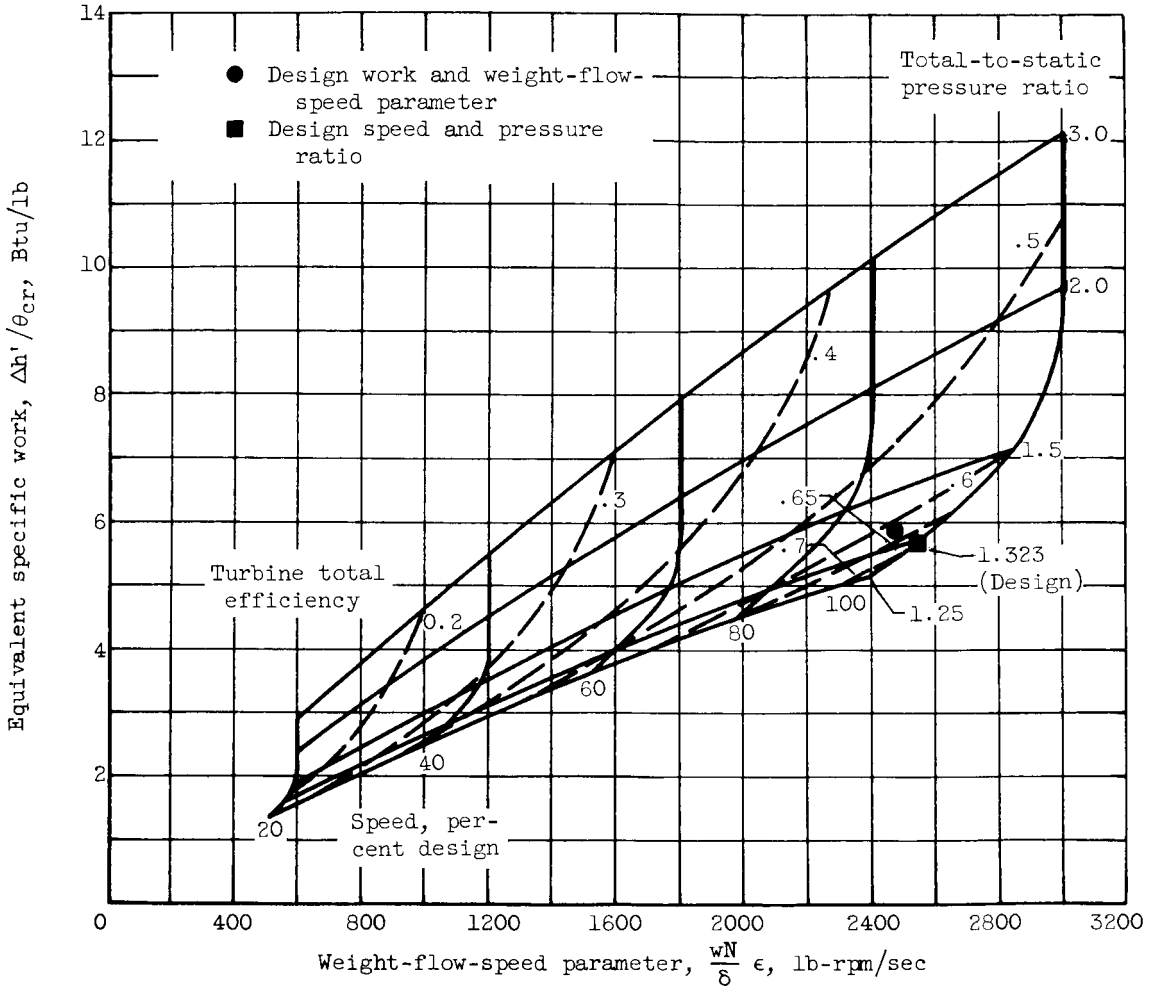

Figure 6. - Performance of first stage of eight-stage turbine in nitrogen.

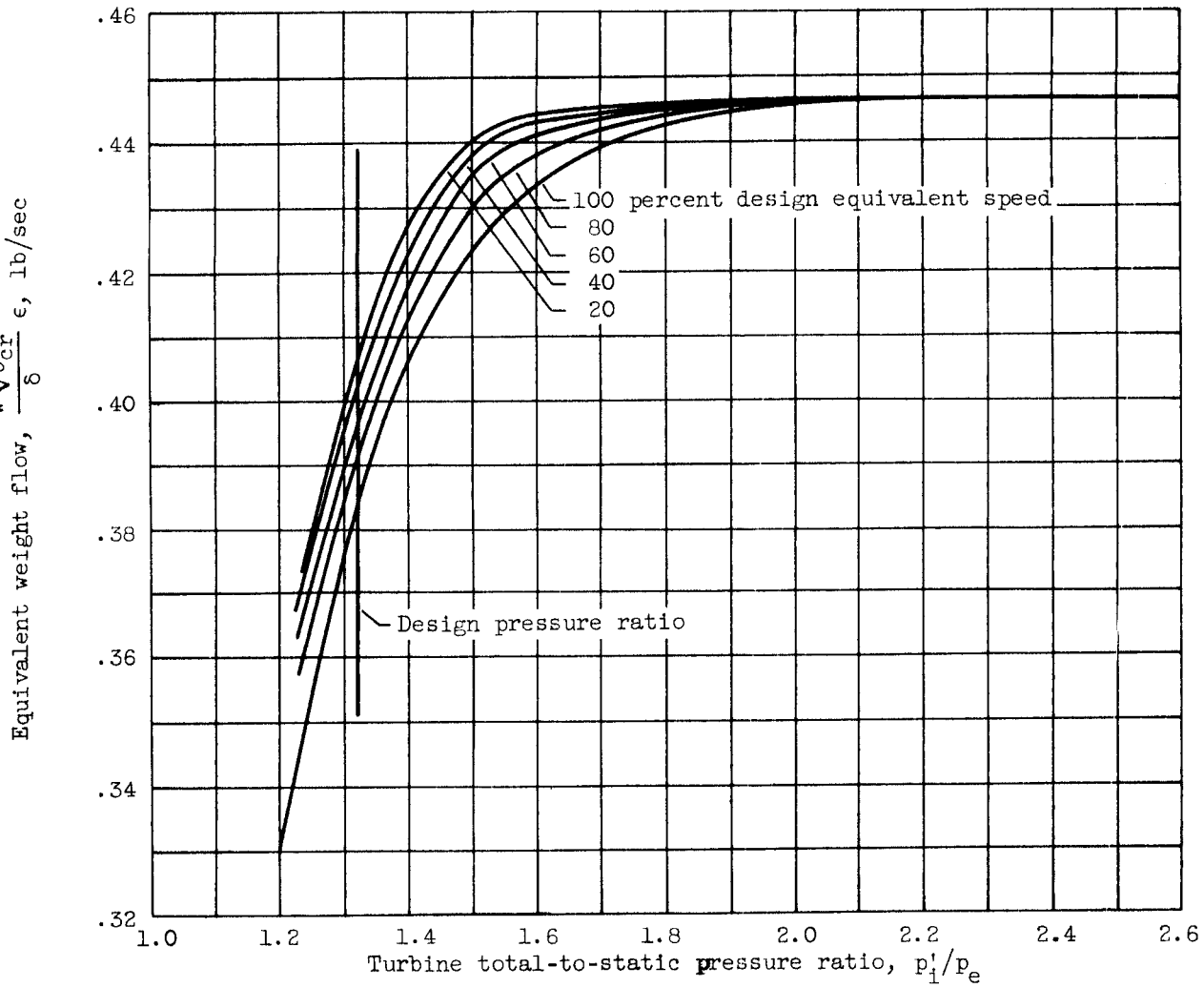

Figure 7. - Variation in weight flow with pressure ratio for operation of first stage in cold nitrogen.

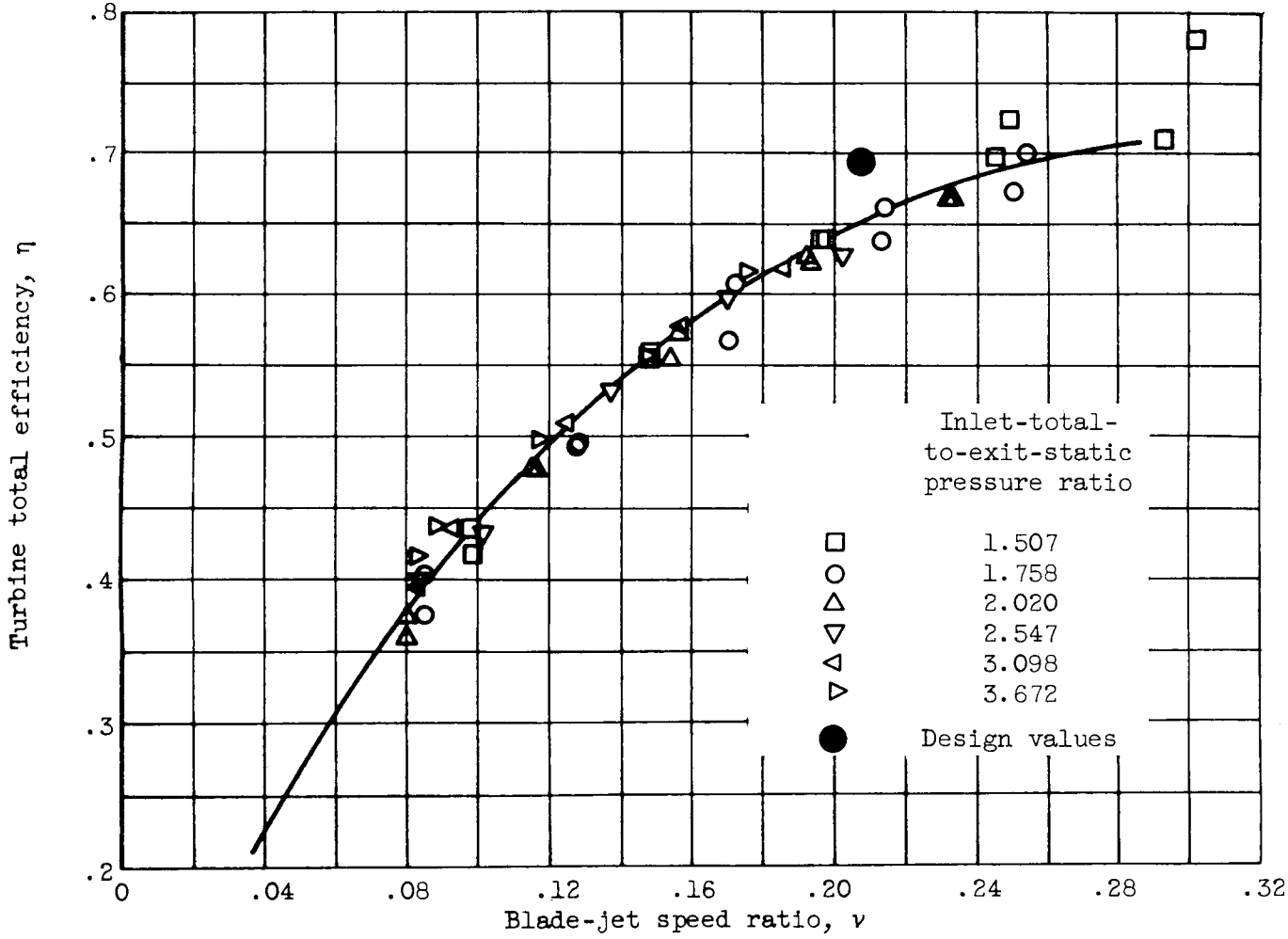

(a) In cold nitrogen.

Figure 8. - Turbine total efficiency variation for operation of first two stages.

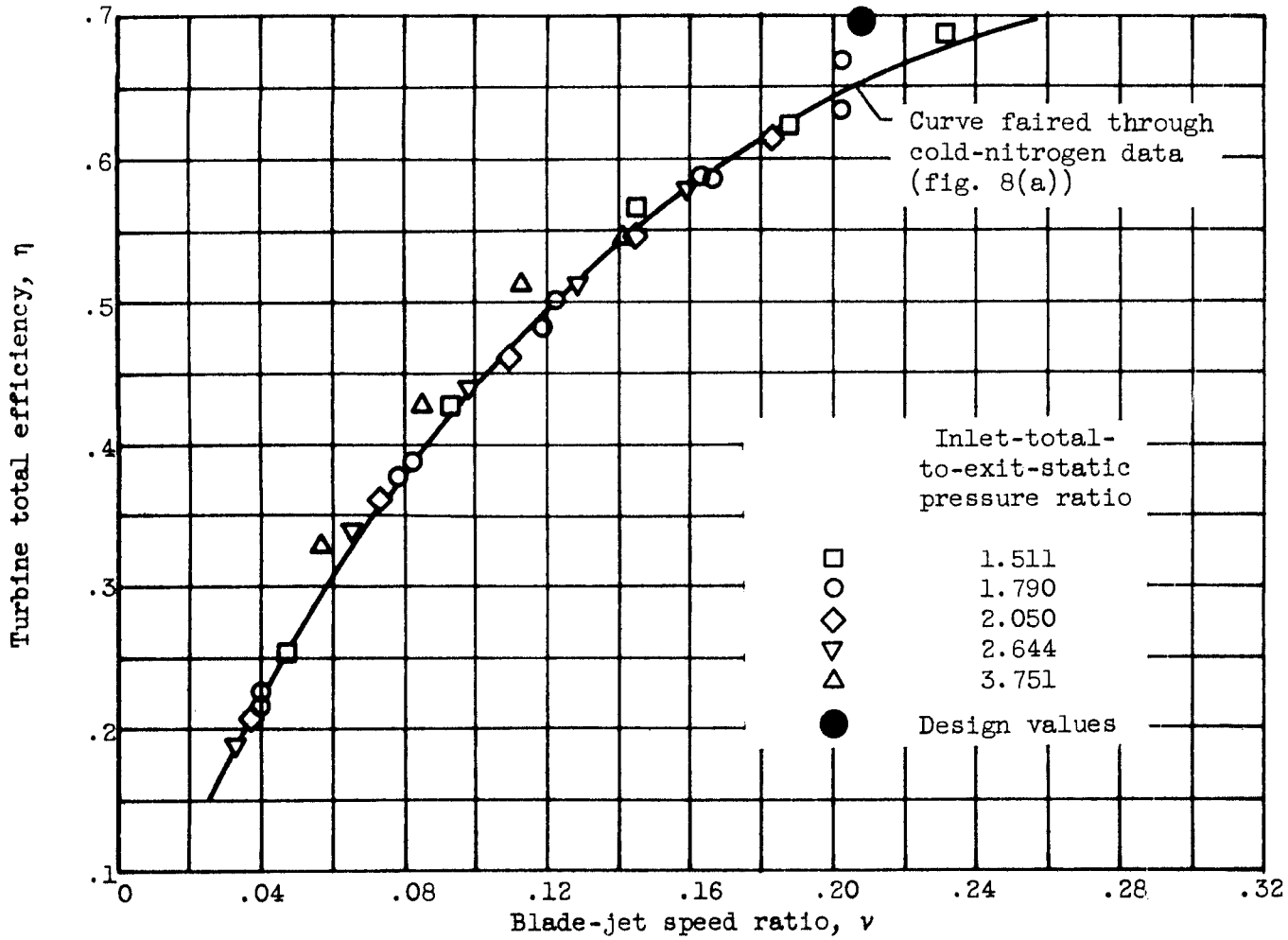

(b) In cold hydrogen.

Figure 8. - Concluded. Turbine total efficiency variation for operation of first two stages.

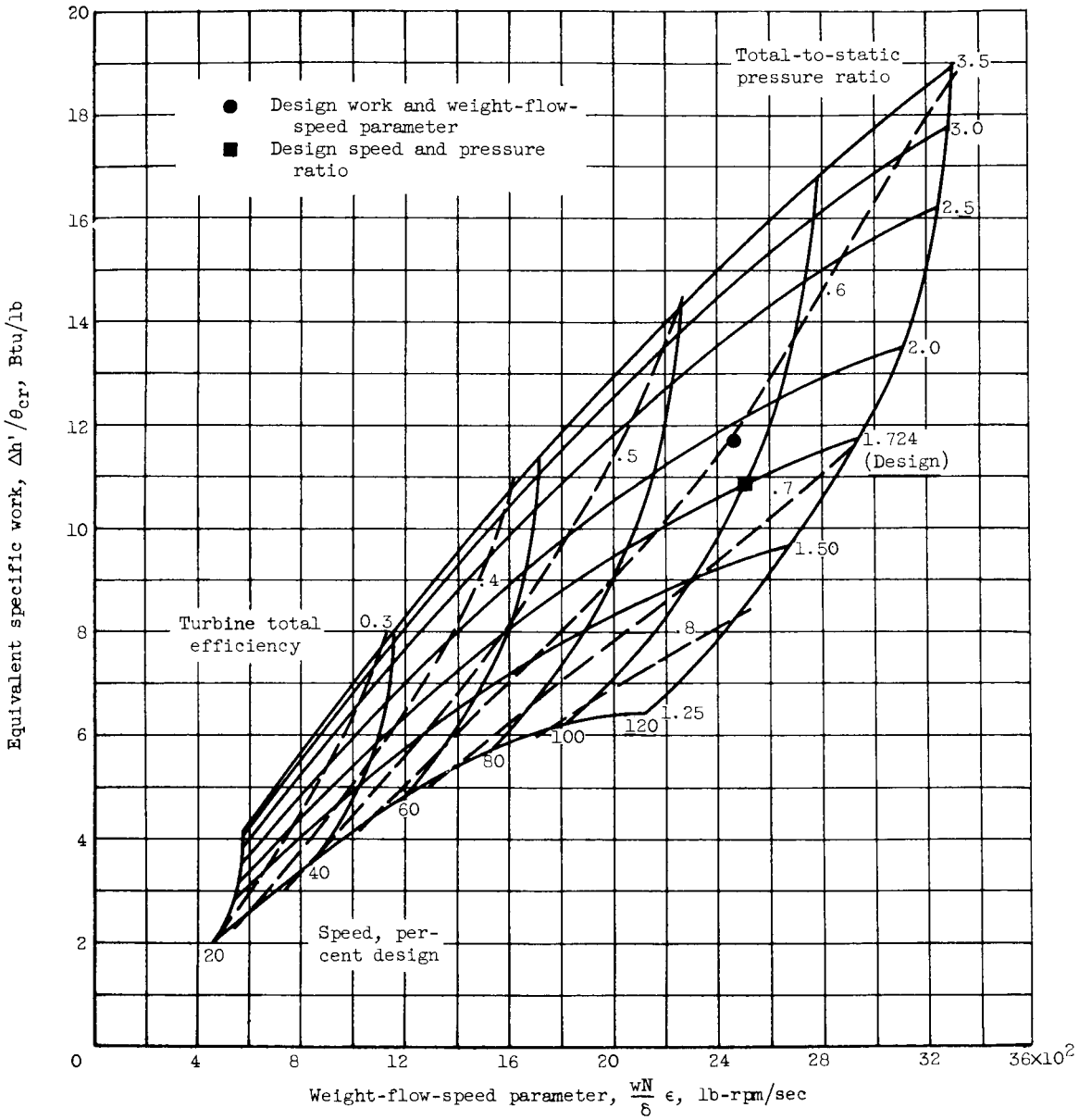

Figure 9. - Performance of first two stages of eight-stage turbine in nitrogen.

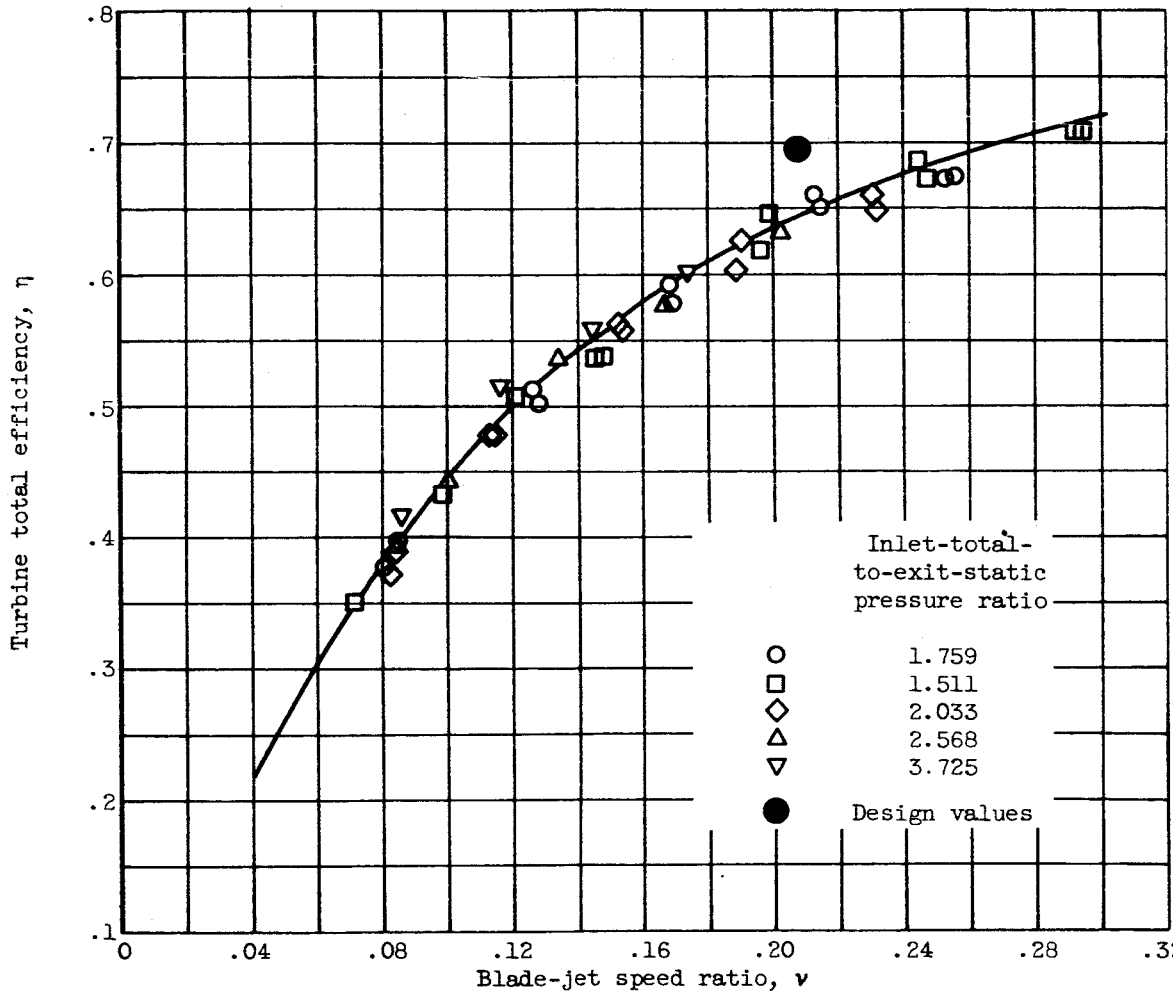

(a) In cold nitrogen.

Figure 10. - Turbine total efficiency variation for operation of first two stages with modified interstage seal.

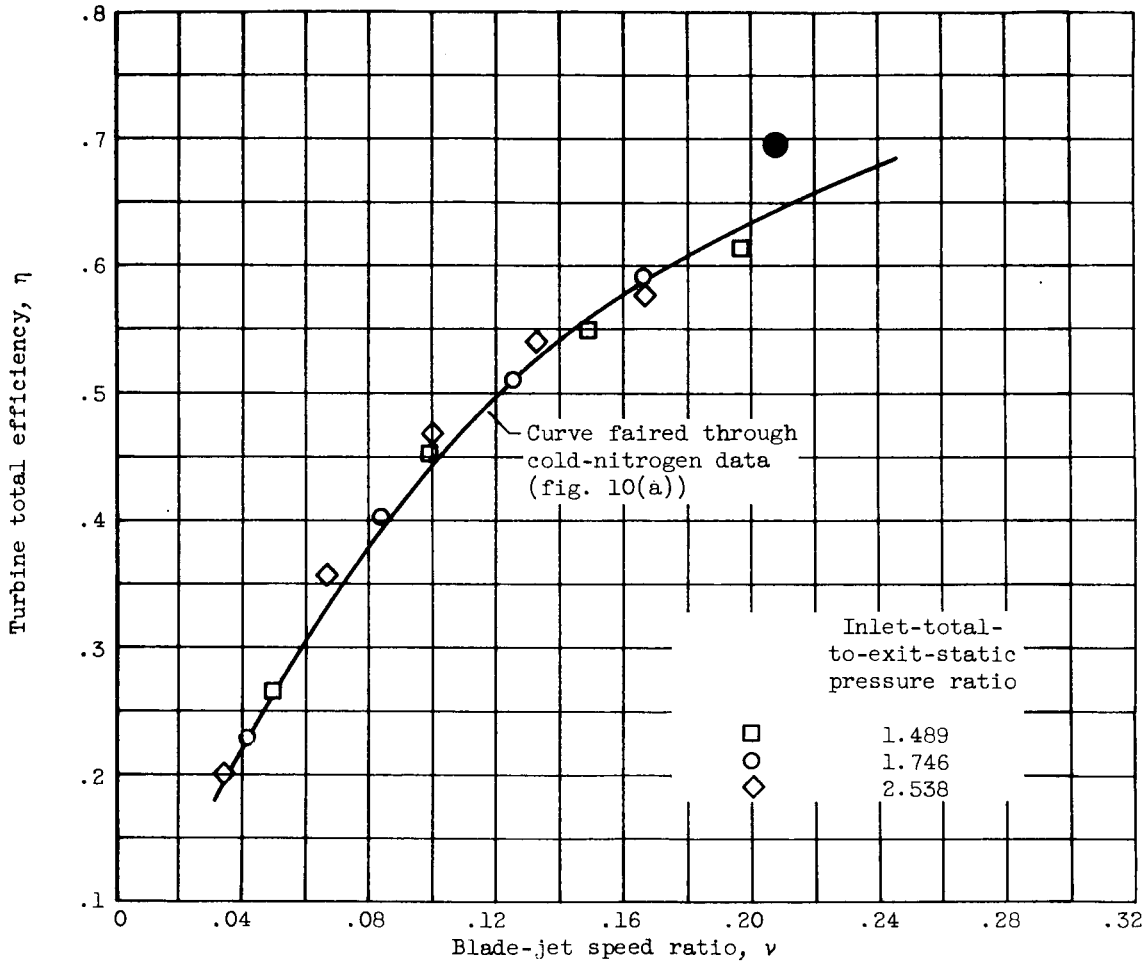

(b) In cold hydrogen.

Figure 10. - Concluded. Turbine total efficiency variation for operation of first two stages with modified interstage seal.